FERMILAB-PUB-06-491-E

Study of the $D^0 \to \pi^-\pi^+\pi^-\pi^+$ decay.

J. M. Link and P. M. Yager

University of California, Davis, CA 95616

J. C. Anjos, I. Bediaga, C. Castromonte, A. A. Machado, J. Magnin,
A. Massafferri, J. M. de Miranda, I. M. Pepe, E. Polycarpo, and A. C. dos Reis

Centro Brasileiro de Pesquisas Físicas, Rio de Janeiro, RJ, Brazil

S. Carrillo, E. Casimiro, E. Cuautle, A. Sánchez-Hernández, C. Uribe, and F. Vázquez

CINVESTAV, 07000 México City, DF, Mexico

L. Agostino, L. Cinquini, J. P. Cumalat, V. Frisullo, B. O'Reilly, I. Segoni, and K. Stenson

University of Colorado, Boulder, CO 80309

J. N. Butler, H. W. K. Cheung, G. Chiodini, I. Gaines, P. H. Garbincius, L. A. Garren,
E. Gottschalk, P. H. Kasper, A. E. Kreymer, R. Kutschke, and M. Wang

Fermi National Accelerator Laboratory, Batavia, IL 60510

L. Benussi, S. Bianco, F. L. Fabbri, and A. Zallo

Laboratori Nazionali di Frascati dell'INFN, Frascati, Italy I-00044

M. Reyes

University of Guanajuato, 37150 Leon, Guanajuato, Mexico

C. Cawlfield, D. Y. Kim, A. Rahimi, and J. Wiss

University of Illinois, Urbana-Champaign, IL 61801

R. Gardner and A. Kryemadhi

Indiana University, Bloomington, IN 47405

Y. S. Chung, J. S. Kang, B. R. Ko, J. W. Kwak, and K. B. Lee

Korea University, Seoul, Korea 136-701

K. Cho and H. Park

Kyungpook National University, Taegu, Korea 702-701

G. Alimonti, S. Barberis, M. Boschini, A. Cerutti, P. D'Angelo, M. DiCorato,
P. Dini, L. Edera, S. Erba, P. Inzani, F. Leveraro, S. Malvezzi, D. Menasce,
M. Mezzadri, L. Moroni, D. Pedrini, C. Pontoglio, F. Prelz, M. Rovere, and S. Sala
INFN and University of Milano, Milano, Italy

T. F. Davenport III
University of North Carolina, Asheville, NC 28804

V. Arena, G. Boca, G. Bonomi, G. Gianini, G. Liguori, D. Lopes Pegna,
M. M. Merlo, D. Pantea, S. P. Ratti, C. Riccardi, and P. Vitulo
Dipartimento di Fisica Nucleare e Teorica and INFN, Pavia, Italy

C. Göbel and J. Otalora
Pontifícia Universidade Católica, Rio de Janeiro, RJ, Brazil

H. Hernandez, A. M. Lopez, H. Mendez, A. Paris, J. Quinones, J. E. Ramirez, and Y. Zhang
University of Puerto Rico, Mayaguez, PR 00681

J. R. Wilson
University of South Carolina, Columbia, SC 29208

T. Handler and R. Mitchell
University of Tennessee, Knoxville, TN 37996

D. Engh, M. Hosack, W. E. Johns, E. Luiggi, M. Nehring,
P. D. Sheldon, E. W. Vaandering, and M. Webster
Vanderbilt University, Nashville, TN 37235

M. Sheaff
University of Wisconsin, Madison, WI 53706

(Dated: January 2, 2007)

Abstract

Using data from the FOCUS (E831) experiment at Fermilab, we present new measurements for the Cabibbo-suppressed decay mode $D^0 \to \pi^-\pi^+\pi^-\pi^+$. We measure the branching ratio $\Gamma(D^0 \to \pi^+\pi^-\pi^+\pi^-)/\Gamma(D^0 \to K^-\pi^+\pi^-\pi^+) = 0.0914 \pm 0.0018 \pm 0.0022$. An amplitude analysis has been performed, a first for this channel, in order to determine the resonant substructure of this decay mode. The dominant component is the decay $D^0 \to a_1(1260)^+\pi^-$, accounting for 60% of the decay rate. The second most dominant contribution comes from the decay $D^0 \to \rho(770)^0\rho(770)^0$, with a fraction of 25%. We also study the $a_1(1260)$ line shape and resonant substructure. Using the helicity formalism for the angular distribution of the decay $D^0 \to \rho(770)^0\rho(770)^0$, we measure a longitudinal polarization of $P_L = (71 \pm 4 \pm 2)\%$.

PACS numbers: 13.25Ft,13.30Eg,13.87Fh

I. INTRODUCTION

Hadronic decays of charm mesons are an important tool for understanding the dynamics of the strong interaction in the low energy regime. Hadronic decays of D mesons typically have a rich resonant structure and a small nonresonant component. Scalar mesons are abundant products of three-body decays which have a pair of identical pions in the final state. Due to these features, three-body decays of D mesons have been extensively used to study the $\pi\pi$ and $K\pi$ systems, with emphasis on the S-wave component of their amplitudes and on the scalar resonances [1–5]. With D decays one can continuously cover the $\pi\pi$ and $K\pi$ mass spectra from threshold up to 1.7 GeV/c^2 ($M_D - m_\pi$), filling the existing gaps between the K_{e4} [6] and the CERN-Münich data [7], in the $\pi\pi$ case, and between threshold and 825 MeV/c^2, where the LASS data [8] on $K\pi$ scattering start. Another interesting feature of D decays is that the bulk of the hadronic decay width can be described in terms of simple tree-level quark diagrams. There seems to be, at least for the vector, axial-vector and tensor mesons, a strong correlation between the final state quarks — the spectator valence quark plus the ones resulting from the weak decay of the c quark — and the quark content of the observed resonances in the intermediate states. This connection allows some insights on the nature of light mesons. The information provided by D decays is, therefore, complementary to that of traditional scattering experiments.

Much less information is available concerning the $\pi\pi\pi/K\pi\pi$ systems and the axial-vector resonances. The picture emerging from many different Dalitz plot analyses of D decays reveals a well defined pattern: final states that can be associated with a simple spectator amplitude (W-radiation), in which the virtual W couples to a vector or axial-vector meson, have large branching fractions compared to final states in which the W is coupled to a pseudo-scalar meson. Following this pattern, one expects the $a_1(1260)^+\pi^-$ channel to be the dominant resonant component of the $D^0 \to \pi^-\pi^+\pi^-\pi^+$ decay (charge conjugation is always implied, unless stated otherwise). This decay, therefore, can be used to study the resonant substructure of the axial-vector meson $a_1(1260)$, as well as its line shape, from threshold up to 1.72 GeV/c^2.

In the study of light mesons from D decays there is one potential difficulty: in hadronic decays the $\pi\pi$ and $K\pi$ pairs, as well as the $\pi\pi\pi/K\pi\pi$ systems, are part of a few-body strongly interacting system. In principle one must account for final state interactions (FSI)

between all decay particles. It is still an open question whether the FSI are strong enough in three-body decays to distort the pure $\pi\pi/K\pi$ scattering amplitudes. In any case, the effects of the FSI should become more important as the number of final state particles increases.

Most amplitude analyses employ the so called isobar model: a coherent sum of resonant amplitudes weighted by constant complex coefficients. The constant phases account for re-scattering effects between the isobar and the other decay particles. This approach to FSI may be sufficient in some cases, but may be too simplistic in four-body decays. In the most general case, the FSI would depend on energy, with a smooth variation across the phase space. A correction to the isobar model would then be necessary in order to incorporate the energy dependent FSI. As we will show, the energy dependent FSI can probably not be ignored in four-body decays of D mesons.

There is an additional motivation for the study of four-body D meson decays. Charmless decays of B mesons are a promising tool for the study of CP violation. In particular, the decays $B \to \rho\rho$ have been used to extract the CKM angle α [9–12]. The $B \to a_1(1260)\pi$ mode, however, also leads to the same $\pi\pi\pi\pi$ final state. The $B^0 \to a_1(1260)^-\pi^+$ channel has a branching fraction which is one order of magnitude larger than that of $B^0 \to \rho^0\rho^0$ [13, 14]. There is no measurement of the $B^\pm \to a_1(1260)^\pm\pi^0$ branching ratio, but since this decay proceeds mainly via the same tree-level W radiation amplitude as that of the $\rho^\pm\rho^0$ channel, one expects these two modes to have comparable rates. The $B \to a_1(1260)\pi$ decay, thus, accounts for a large fraction of the $B \to \pi\pi\pi\pi$ decay, and a full amplitude analysis would be necessary in order to isolate the $B \to \rho\rho$ contribution, as in the case of the $D^0 \to \pi^-\pi^+\pi^-\pi^+$ decay. All the systematics — form factors, resonance line shapes, representation of the S-wave components, angular distributions, FSI, etc. — are common to both decays. One can think of the $D^0 \to \pi^-\pi^+\pi^-\pi^+$ decay as a prototype of the $B \to \pi\pi\pi\pi$ decay.

In this paper, we present a new measurement of the relative branching ratio (BR) $\Gamma(D^0 \to \pi^-\pi^+\pi^-\pi^+)/\Gamma(D^0 \to K^-\pi^+\pi^-\pi^+)$ using data from the FOCUS experiment. For the first time an amplitude analysis has been performed to determine the $D^0 \to \pi^-\pi^+\pi^-\pi^+$ resonant substructure.

II. THE FOCUS EXPERIMENT

FOCUS, an upgraded version of E687 [15], is a charm photo-production experiment which collected data during the 1996–97 fixed target run at Fermilab. Electron and positron beams (typically with 300 GeV endpoint energy) obtained from the 800 GeV Tevatron proton beam produce, by means of bremsstrahlung, a photon beam which interacts with a segmented BeO target [16]. The mean photon energy for reconstructed charm events is ~ 180 GeV. A system of three multi-cell threshold Čerenkov counters performs the charged particle identification, separating kaons from pions up to a momentum of 60 GeV/c. Two systems of silicon micro-vertex detectors are used to track particles: the first system consists of 4 planes of micro-strips interleaved with the experimental target [17] and the second system consists of 12 planes of micro-strips located downstream of the target. These high resolution detectors allow the identification and separation of charm primary (production) and secondary (decay) vertices. The charged particle momentum is determined by measuring the deflections in two magnets of opposite polarity through five stations of multi-wire proportional chambers.

III. THE $D^0 \to \pi^-\pi^+\pi^-\pi^+$ SAMPLE

The final states are selected using a candidate driven vertex algorithm [15]. To minimize systematic errors on the measurements of the branching ratio, we use identical vertex cuts on the signal and normalizing mode.

Secondary vertices are formed from the four candidate tracks. The momentum of the resultant D^0 candidate is used as a *seed* track to intersect other reconstructed tracks and to search for a primary vertex. The confidence levels of both vertices are required to be greater than 1%. Once the production and decay vertices are determined, the distance L between the vertices and its uncertainty σ_L are computed. The ratio L/σ_L is the most important variable for separating charm events from non-charm prompt backgrounds. Signal quality is further enhanced by cutting on the isolation variables, *Iso1* and *Iso2*. The isolation variable *Iso1* requires that the tracks forming the D candidate vertex have a confidence level smaller than the cut to form a vertex with the tracks from the primary vertex. The *Iso2* variable requires that all remaining tracks not assigned to the primary and secondary vertex have a confidence level smaller than the cut to form a vertex with the D candidate daughters.

In addition, we require the secondary vertex to lie outside of the segmented targets (*O*ut-*o*f-*M*aterial cut, or *OoM*), in order to reduce contamination due to secondary interactions. The *OoM* variable is actually the the distance between the secondary vertex and the edge of the nearest target segment divided by the uncertainty on the secondary vertex location. We have also applied a cut on $\mathrm{vtx}_{\mathrm{score}}$, a variable built from the *OoM*, $L\,/\,\sigma_L$ and the confidence level of the secondary vertex, in order to explore the correlations between these variables. Each of these variables is normalized to its maximum value, so $\mathrm{vtx}_{\mathrm{score}}$ ranges from 0 to 1. This cut allows us to further reduce the background without applying tighter cuts on each of these variables. The set of cuts that yield the $D^0 \to \pi^-\pi^+\pi^-\pi^+$ signal with the best statistical significance is $L\,/\,\sigma_L > 10$, *Iso1* and *Iso2* $< 10\%$, $\mathrm{vtx}_{\mathrm{score}} > 0.15$ and $OoM > 1$.

The only difference in the selection criteria between the $D^0 \to \pi^-\pi^+\pi^-\pi^+$ and $D^0 \to K^-\pi^+\pi^-\pi^+$ decay modes lies in the particle identification cuts. The Čerenkov identification cuts used in FOCUS are based on likelihood ratios between the various particle identification hypotheses. These likelihoods are computed for a given track from the observed firing response (on or off) of all the cells that are within the track's ($\beta = 1$) Čerenkov cone for each of our three Čerenkov counters. The product of all firing probabilities for all the cells within the three Čerenkov cones produces a χ^2-like variable $W_i = -2\log(\mathrm{Likelihood})$ where i ranges over the electron, pion, kaon, and proton hypotheses [18]. The kaon track is required to have $\Delta_K = W_\pi - W_K > 3$, and all pion tracks are required to be separated by less than 5 from the best hypothesis, that is $\Delta_\pi = W_{\mathrm{min}} - W_\pi > -5$.

Using the set of selection cuts just described, we obtain the invariant mass distribution for $\pi^-\pi^+\pi^-\pi^+$ shown in Fig. 1. Although the Čerenkov cuts considerably reduce the reflection peak (from $D^0 \to K^-\pi^+\pi^-\pi^+$) to the left of the signal peak, there is still a large distortion of the background due to this surviving contamination. The $\pi^-\pi^+\pi^-\pi^+$ mass plot is fit with a function that includes two Gaussians with the same mean but different sigmas to take into account the variation in momentum resolution of our spectrometer as a function of particle momentum [15], and two exponential functions for the combinatorial background and for the $D^0 \to K^-\pi^+\pi^-\pi^+$ reflection. A log-likelihood fit gives a signal of 6360 ± 115 $D^0 \to \pi^-\pi^+\pi^-\pi^+$ events.

The large statistics $K^-\pi^-\pi^+\pi^+$ mass plot is also fit with two Gaussians with the same mean and different sigmas plus a second-order polynomial for the background. A log-likelihood fit gives a signal of 54156 ± 267 $D^0 \to K^-\pi^-\pi^+\pi^+$ events.

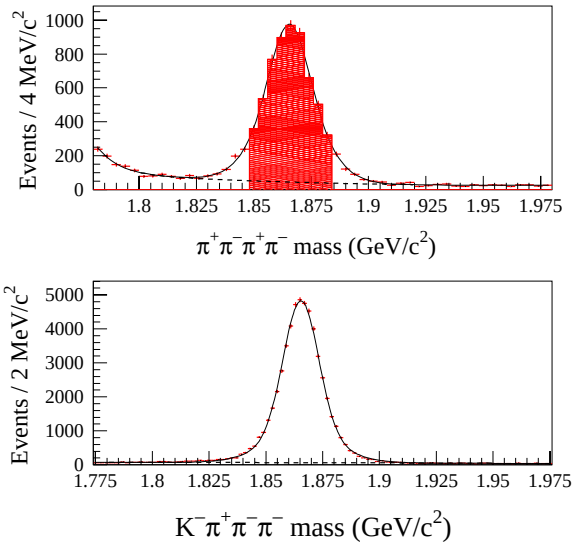

FIG. 1: Invariant mass distributions used to determine the ratio of branching fractions. The upper plot is the $\pi^-\pi^+\pi^-\pi^+$ signal; the lower plot is the normalizing channel $K^-\pi^+\pi^-\pi^+$. The fits (solid curves) are explained in the text; the dashed line shows the background. The hatched area on the $\pi^-\pi^+\pi^-\pi^+$ signal corresponds to the events used in the amplitude analysis.

IV. RELATIVE BRANCHING RATIO

The evaluation of relative branching ratios requires yields from the fits to be corrected for detector acceptance and efficiency. These differ among the various decay modes, depending on the Q values and Čerenkov identification efficiency.

From the Monte Carlo simulations, we compute the relative efficiencies (with statistical error only):

$$\frac{\epsilon(D^0 \to K^-\pi^+\pi^-\pi^+)}{\epsilon(D^0 \to \pi^-\pi^+\pi^-\pi^+)} = 0.7891 \pm 0.0004. \quad (1)$$

Using the previous results, we obtain the following value for the branching ratio:

$$\frac{\Gamma(D^0 \to \pi^-\pi^+\pi^-\pi^+)}{\Gamma(D^0 \to K^-\pi^+\pi^-\pi^+)} = 0.0914 \pm 0.0018. \quad (2)$$

Systematic uncertainties on the branching ratio measurement may come from different sources. We consider three independent contributions to the systematic uncertainty: the

split sample component, the *fit variant* component, and the component due to the particular choice of the vertex and Čerenkov cuts.

The *split sample* component takes into account the systematics introduced by a residual difference between data and Monte Carlo, due to a possible mismatch in the reproduction of the D^0 momentum and the changing experimental conditions of the spectrometer during data collection. This component has been determined by splitting data into four independent subsamples, according to the D^0 momentum range (high and low momentum) and the configuration of the vertex detector, that is, before and after the insertion of the upstream silicon system. A technique, employed in FOCUS and modeled after the *S-factor method* from the Particle Data Group [19], was used to try to separate true systematic variations from statistical fluctuations. The branching ratio is evaluated for each of the four statistically independent subsamples and a *scaled error* $\tilde{\sigma}$ (that is the errors are boosted when $\chi^2/(N-1) > 1$) is calculated. The *split sample* error $\sigma_{\rm split}$ is defined as the difference in quadrature between the statistical error returned by the fit on the unsplit data set, σ_{stat}, and the scaled error, if the scaled error exceeds the statistical error, $\sigma_{\rm split} = \sqrt{\tilde{\sigma}^2 - \sigma_{stat}^2}$.

Another possible source of systematic uncertainty is the *fit variant*. This component is computed by varying, in a reasonable manner, the fitting conditions for the whole data set. In our study we fixed the widths of the Gaussian to the values obtained by the Monte Carlo simulation, we changed the background parametrization (varying the degree of the polynomial), and we use one Gaussian instead of two. The latter is the dominant contribution to the *fit variant* error. Finally the variation of the computed efficiencies, both for $D^0 \to \pi^-\pi^+\pi^-\pi^+$ and the normalizing decay mode, due to the different resonant substructure simulated in the Monte Carlo has been taken into account. The BR values obtained by these variants are all *a priori* equally likely, therefore this uncertainty can be estimated by the *r.m.s.* of the measurements.

We estimate the cut component systematic error by varying vertex and particle identification cuts one at a time. We varied the confidence level of the secondary vertex from 1% to 50%, *Iso1* and *Iso2* from 10^{-6} to 1, $L\,/\,\sigma_L$ from 6 to 20, Δ_π from -6 to -2, and $\mathrm{vtx}_{\rm score}$ from 0 to 0.2. Analogously to the *fit variant*, the cut component is estimated using the standard deviation of the several sets of cuts. Actually, this is an overestimate of the cut component because the statistics of the cut samples are different.

Finally, adding in quadrature the three components, we get the final systematic errors

TABLE I: Contributions to the systematic uncertainties of the branching ratio $\Gamma(D^0 \to \pi^-\pi^+\pi^-\pi^+)/\Gamma(D^0 \to K^-\pi^+\pi^-\pi^+)$.

Source	Systematic error
Split sample	0.0010
Fit Variant	0.0012
Set of cuts	0.0016
Total systematic error	0.0022

TABLE II: Comparison with other experiments.

Experiment	$\Gamma(D^0 \to \pi^-\pi^+\pi^-\pi^+)/\Gamma(D^0 \to K^-\pi^+\pi^-\pi^+)$	Events
FOCUS (this result)	$0.0914 \pm 0.0018 \pm 0.0022$	6360 ± 115
CLEO-c [20]	$0.097 \pm 0.002 \pm 0.003$	7331 ± 130
BES [21]	$0.079 \pm 0.018 \pm 0.005$	162 ± 20
E687 [22]	$0.095 \pm 0.007 \pm 0.002$	814 ± 26

which are summarized in Table I.

The final result is shown in Table II along with a comparison with previous measurements.

V. AMPLITUDE ANALYSIS

A fully coherent amplitude analysis was performed in order to determine the resonant substructure of the $D^0 \to \pi^-\pi^+\pi^-\pi^+$ decay. This is, to our knowledge, the first such measurement for this channel. The amplitude analysis was performed in the framework of the isobar model on a sample of 6153 events, corresponding to the hatched area in Fig. 1 (events with $m_{4\pi}$ within 20 MeV/c^2 of the D^0 mass).

A. A model for the $D^0 \to \pi^-\pi^+\pi^-\pi^+$ decay

The decay mode $D^0 \to \pi^-\pi^+\pi^-\pi^+$ is Cabibbo-suppressed and may proceed through many intermediate resonant states. Considering only tree-level amplitudes, we expect contributions from two-body decays such as $D \to R\pi$, $D \to RR$, and from three-body nonresonant

decays $D \to R\pi\pi$ ($R = f_0(600)$ or σ, $\rho(770)^0$, $f_0(980)$, $f_2(1270)$, $f_0(1370)$, $\rho(1450)^0$). Including all possible contributions, one could have over twenty different resonant amplitudes leading to the $\pi^-\pi^+\pi^-\pi^+$ final state.

The $\pi^-\pi^+\pi^-\pi^+$ final state could also result from a nonresonant decay. Usually the nonresonant component is assumed to be uniform, but this may not be a reasonable assumption even in the simpler case of three-body decays [23]. To our knowledge there is no phenomenological model for a non-uniform nonresonant amplitude in four-body decays.

The existence of many possible intermediate states leading to the $\pi^-\pi^+\pi^-\pi^+$ final state makes the amplitude analysis of this decay very challenging. Many of these intermediate states involve broad resonances that populate the whole phase space. A model having a large number of overlapping amplitudes gives rise to large interference terms which are difficult to control in a five-dimensional space. The presence of these interference terms is easily detected when the sum of decay fractions greatly exceeds 100%. In such cases many local minima exist in the parameter space, with very similar likelihood values. With such a model one may find a mathematical solution to the fit problem, losing, however, the physical meaning of it. An additional difficulty comes from the fact that in the $\pi^-\pi^+\pi^-\pi^+$ final state there are two pairs of identical pions and therefore amplitudes must be Bose-symmetrized. In the chain $D^0 \to a_1(1260)^+\pi^-$, $a_1(1260)^+ \to \rho^0\pi^+$, $\rho^0 \to \pi^+\pi^-$, for instance, one can combine the four pions in eight possible ways. Angular distributions, a clean signature of specific modes, tend to be smeared out by the Bose-symmetrization. This could be minimized using flavor tagging, since a large fraction of the D^0 comes from the decay $D^{*\pm} \to D^0(\overline{D}^0)\pi^\pm$. In our case that would reduce the sample size by a factor of five. Finally, as the number of final state particles increases the more important the final state interactions tend to be. The FSI may play a significant role in the $D^0 \to \pi^-\pi^+\pi^-\pi^+$ decay. Unfortunately this is a very difficult problem to deal with, even with a phenomenological approach.

The strategy adopted in this analysis is to start with a set of amplitudes corresponding to modes that are expected to be dominant. Once a stable solution is achieved, modes with marginal contributions are replaced by other ones, until a final set is reached.

We built a baseline mode guided by the $\pi^-\pi^+$ projections, by MC simulation of the different channels and by our own experience. The $\pi^-\pi^+$ mass projections are shown in Fig. 2. The plot in Fig. 2(a) has four entries per event, corresponding to the four different $\pi^-\pi^+$ combinations one could form in each event. We adopt the particle labeling $D^0 \to \pi_1^-\pi_2^+\pi_3^-\pi_4^+$,

so the identical particles are π_1/π_3 and π_2/π_4. In our sample we do not distinguish between D^0 and $\overline{D}^0$, and the like charge pions are randomized to avoid any ordering with respect to their momenta. Consequently, all four pions have the same momentum distribution, making the four $\pi^-\pi^+$ mass projections indistinguishable.

One can form two combinations of $\pi^-\pi^+$ pairs, $\pi_1^-\pi_2^+/\pi_3^-\pi_4^+$ or $\pi_1^-\pi_4^+/\pi_2^-\pi_3^+$. One can plot the highest and lowest $\pi^-\pi^+$ invariant mass for each pair combination. These are shown in Fig. 2(b)-(c), respectively. In these plots there are two entries per event.

The $\rho(770)^0$ is clearly the dominant $\pi^-\pi^+$ resonance, although other resonances, like the σ, $f_0(980)$ and $f_2(1270)$ may also be present, even without leaving a clear signature in the $\pi^-\pi^+$ mass projection. The $\rho(770)^0$ signal could originate from the decay of the axial-vector meson $a_1(1260)$, from the decay of the type $D^0 \to \rho^0\rho^0$, $D^0 \to \rho^0 R$, or even from $D^0 \to \rho^0\pi^+\pi^-$. Figure 2(d) shows the $\pi^-\pi^+$ projection of Monte Carlo (MC) simulations of the decay $D^0 \to a_1(1260)^+\pi^-$, with the a_1 decaying to $\rho^0\pi^+$ (S- and D-wave) and to $\sigma\pi^+$.

Our baseline model includes contributions of three types. The first type is the $D^0 \to a_1(1260)^+\pi^-$ chain. For the $a_1(1260)$ resonant substructure, we consider three channels: $a_1^+ \to \rho(770)^0\pi^+$, the $\rho^0\pi^+$ being in a dominant S-wave state with a small D-wave component, plus $a_1^+ \to \sigma\pi^+$. The second type of contribution is the $D^0 \to \rho^0\rho^0$ decay, in three possible helicity states. Finally, we consider decays of the type $D^0 \to R\pi^+\pi^-$, with $R = \sigma, \rho^0, f_0(980)$ and $f_2(1270)$.

B. Formalism

The formalism used in this amplitude analysis is a straightforward extension to four-body decays of the usual Dalitz plot fit technique. The $D^0 \to \pi^-\pi^+\pi^-\pi^+$ signal amplitude is represented by a coherent sum of individual amplitudes, each corresponding to a possible intermediate state and weighted by constant complex coefficients c_k, $\mathcal{A} = \sum c_k A_k$. The background amplitude is represented by an incoherent sum of amplitudes corresponding to the different types of background events.

A likelihood function is built from the signal and background amplitudes, incorporating detector resolution effects and acceptance correction. The optimum set of constants c_k, the only unknowns, is obtained by an unbinned maximum likelihood fit. The background amplitude is kept fixed during the fit procedure.

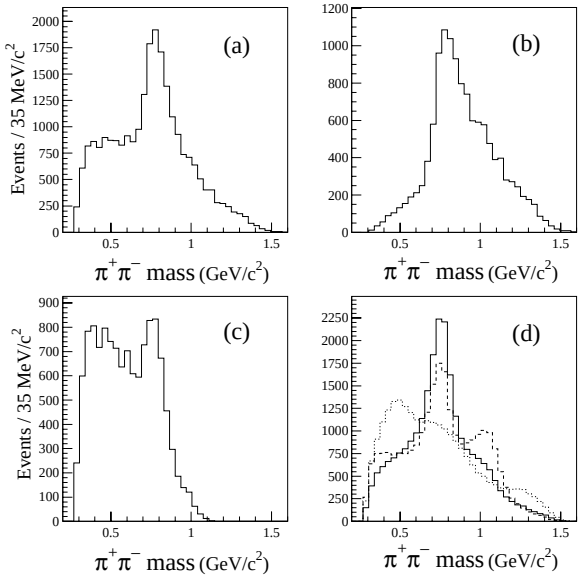

FIG. 2: Invariant mass distribution for $\pi^-\pi^+$. (a) All four $\pi^-\pi^+$ combinations; (b) the $\pi^-\pi^+$ combinations with highest mass; (c) the $\pi^-\pi^+$ combinations with lowest mass; (d) MC simulation of the $\pi^-\pi^+$ mass distribution for $D^0 \to a_1(1260)^+\pi^-$: the solid line corresponds to the $a_1^+ \to \rho(770)^0\pi^+$ S-wave, the dashed line is the $a_1^+ \to \rho(770)^0\pi^+$ D-wave, and the dotted line is $a_1^+ \to \sigma\pi^+$.

1. Phase space

The kinematics of the $D^0 \to \pi^-\pi^+\pi^-\pi^+$ decay is unambiguously determined by five degrees of freedom. We choose a set of five two-body invariant masses squared — the four different $\pi^-\pi^+$ combinations, $s_{12}, s_{14}, s_{23}, s_{34}$ plus s_{13} — to define an event in the five-dimensional phase space. Any kinematic variable, like acoplanarity and helicity angles or three-body masses, can be easily expressed in terms of this set of invariants. Unlike the case of three-body decays, the phase space density is no longer constant.

2. Signal amplitudes

The amplitudes for the intermediate states, A_i, are phenomenological objects. Each signal amplitude is built as a product of relativistic Breit-Wigner functions (BW), an overall spin amplitude, $\mathcal{M}$, accounting for angular momentum conservation at each decay vertex, and form factors, F_l (l is the orbital angular momentum of the decay vertex), accounting for

the finite hadron size. This is the standard structure for resonant amplitudes (see note of Dalitz plot formalism in [19]). The amplitude for the decay chain $D^0 \to a_1(1260)^+\pi^-$, $a_1(1260)^+ \to \rho^0\pi^+$ (S-wave), $\rho^0 \to \pi^+\pi^-$, is

$$A = F_1^D \times \mathrm{BW}^{a_1} \times F_1^{a_1} \times \mathrm{BW}^{\rho} \times F_1^{\rho} \times \mathcal{M}. \tag{3}$$

The amplitude for the decay chain $D^0 \to \rho_1^0\rho_2^0$, $\rho_1^0 \to \pi^+\pi^-$, $\rho_2^0 \to \pi^+\pi^-$ is

$$A = F_l^D \times \mathrm{BW}^{\rho_1} \times F_1^{\rho_1} \times \mathrm{BW}^{\rho_2} \times F_1^{\rho_2} \times \mathcal{M}, \tag{4}$$

and for the chain $D^0 \to f_2(1270)\pi^+\pi^-$, $f_2(1270) \to \pi^+\pi^-$ the amplitude is

$$A = F_2^D \times \mathrm{BW}^{f_2} \times F_2^{f_2} \times \mathcal{M}. \tag{5}$$

All signal amplitudes are Bose-symmetrized due to the existence of two pairs of identical particles in the final state.

We use the Blatt-Weisskopf damping factors [24] as form factors for vertices involving spin-1 and spin-2 resonances. These form factors have one free parameter, r_R, which is related to the resonance size. All form factors are slowly varying functions of energy. As a systematic check we varied the value of r_R. The fit result is not very sensitive to the value of this parameter in the range $1 < r_R < 5$ GeV^{-1}. The form factor parameter is fixed at $r_R = 3.0$ GeV^{-1}.

For the spin amplitudes we use the Lorentz invariant amplitudes for the decay sequences $D^0 \to a_1^+\pi^-$ and $D \to R\pi^+\pi^-$ (R being a vector or tensor resonance). These Lorentz invariant amplitudes are built using the relativistic tensor formalism [25, 26] which combines particle 4-momenta with polarization vectors in a rotationally invariant way. In vertices involving only the strong interactions, parity conservation imposes an additional constraint. For the decay $D^0 \to \rho^0\rho^0$ the spin amplitudes are written using the helicity formalism. Explicit formulae for the angular distributions are presented in the Appendix.

The relativistic Breit-Wigner representing the $f_2(1270)$ and σ resonances has an energy dependent width, with the approximation $\Gamma_{\pi\pi}(s) = \Gamma_{\mathrm{tot}}(s)$,

$$\mathrm{BW} = \frac{1}{s - s_0 + i\sqrt{s_0}\Gamma_{\mathrm{tot}}(s)}, \tag{6}$$

where

$$\Gamma_{\rm tot}(s) = \Gamma_0 \sqrt{\frac{s_0}{s}} \left(\frac{p^*}{p_0^*}\right)^{2l+1} \frac{F_l^2(p^*)}{F_l^2(p_0^*)}. \quad (7)$$

In the above equations s is the $\pi^+\pi^-$ mass squared, p^* is the break-up momentum of the resonance, s_0 the resonance nominal mass squared, and $p_0^* = p^*(s_0)$.

The ρ^0 line shape is better described when the interference with the $\omega(782)$ is included. In spite of the tiny branching fraction of the $\omega(782) \to \pi^+\pi^-$, the effect of the ρ–ω interference is remarkable and clearly distorts the pure ρ^0 line shape, as one can see by comparing the $\pi^+\pi^-$ with the $\pi^0\pi^\pm$ mass distributions from [28]. In this analysis we use the line shape given by the Crystal Barrel Collaboration [29].

For the $f_0(980)$ we used the Flatté formula [30] of a coupled channel Breit-Wigner function. The $f_0(980)$ parameters — $g_\pi = 0.20 \pm 0.04$, and $g_K = 0.50 \pm 0.20$ and $m_0 = (0.957 \pm 0.008)$ GeV/c^2 — are obtained by a fit to the FOCUS $D_s^+ \to \pi^+\pi^-\pi^+$ Dalitz plot, where the $f_0(980)\pi^+$ is the dominant component.

The $f_2(1270)$ Breit-Wigner parameters are fixed at the PDG values [19], whereas for the σ we used the E791 parameters [1]. It is well known that the σ pole cannot be obtained from a simple Breit-Wigner [27]. Nevertheless, good fits have been obtained by different experiments, in different channels, using Breit-Wigners with similar parameters. There is no consensus on the correct way to parameterize this low mass, broad scalar state. The focus here, however, is not on the σ properties, but on the $a_1(1260)$ line shape, which depends on its resonant substructure. For this purpose it suffices to use the Breit-Wigner formula as an effective representation of a scalar component of the $a_1(1260)$ resonant substructure. In Section VI.D we discuss the sensitivity of the fit results to the values of the σ parameters.

3. The $a_1(1260)$ line shape

One of the main goals of this analysis is to determine the $a_1(1260)$ line shape and its resonant substructure. These are correlated: we need to know the resonant substructure in order to determine the line shape because the resonant substructure defines how the $a_1(1260)$ width, $\Gamma_{\rm tot}^{a_1}(s)$ depends on the $\pi^+\pi^-\pi^+$ mass squared s. Given the functional form of $\Gamma_{\rm tot}^{a_1}(s)$, we represent the a_1 line shape by the same Breit-Wigner formula of Eq. (6). The total width of the $a_1(1260)$ is given by

$$\Gamma^{a_1}_{\rm tot}(s) = \Gamma^{a_1}_{2\pi^0\pi^+}(s) + \Gamma^{a_1}_{2\pi^+\pi^-}(s) + g^2_{K^*K}\Gamma^{a_1}_{K^*K}(s). \quad (8)$$

We assume that $\Gamma^{a_1}_{2\pi^0\pi^+}(s) = \Gamma^{a_1}_{2\pi^+\pi^-}(s)$. The a_1 can also decay to $KK\pi$ via $f_0(980)\pi$ or $K^*(892)K$. The opening of these channels introduces a cusp-like effect in the a_1 width. Since no evidence of the mode $f_0(980)\pi$ has been reported so far, we assume the $KK\pi$ partial width is entirely due to $K^*(892)K$. The value of the coupling constant $g^2_{K^*K}$ is taken from the analysis of the decay $\tau \to \pi^0\pi^0\pi^+\nu_\tau$ by CLEO [31]. The coupling constant $g^2_{K^*K}$ was also measured by the Belle Collaboration [32], which found a value three to five times larger than that measured by CLEO. The uncertainty on the value of $g^2_{K^*K}$ is a source of systematic uncertainty.

The partial width $\Gamma^{a_1}_{2\pi^+\pi^-}(s)$ is obtained by integrating the $\pi^+\pi^-\pi^+$ Dalitz plot,

$$\Gamma^{a_1}_{2\pi^+\pi^-}(s) \propto \frac{1}{s^{3/2}} \int ds_1 ds_2 \left|\mathcal{A}_{a_1}(s_1, s_2)\right|^2, \quad (9)$$

with s_1, s_2 being the invariant mass squared of the two possible $\pi^+\pi^-$ combinations and

$$\mathcal{A}_{a_1}(s_1, s_2) = \sum_{i=1}^{3} c_i A_i(s_1, s_2), \quad (10)$$

where c_i are complex coefficients and $A_i(s_1, s_2)$ the amplitudes for each of the a_1 decay modes. We fix the partial width by demanding that $\Gamma^{a_1}_{2\pi^+\pi^-}(s = s^{a_1}_0) = \Gamma^{a_1}_0$, with $s^{a_1}_0$ and $\Gamma^{a_1}_0$ being real input parameters to be determined.

In practice, we used an iterative procedure: assuming initial values for $s^{a_1}_0$ and $\Gamma^{a_1}_0$, and for the constants c_i, the total width $\Gamma^{a_1}_{\rm tot}(s)$ is computed. Having computed $\Gamma^{a_1}_{\rm tot}(s)$, we perform the five-dimensional fit, which returns new values for the constants c_i; the function $\Gamma^{a_1}_{2\pi^+\pi^-}(s)$ is then recomputed using the same values of $s^{a_1}_0$ and $\Gamma^{a_1}_0$ and the new values of the constants c_i. The process converges after a few iterations. The whole procedure is repeated many times, scanning over the values of s_{a_1} and $\Gamma^{a_1}_0$, until we find the combination that optimizes the fit result.

4. Background

The background composition was determined by inspection of the data on the side band to the right of the D^0 signal in the $\pi^-\pi^+\pi^-\pi^+$ mass spectrum. We consider two types

of background events: random combinations of a $\rho(770)^0$ and a $\pi^-\pi^+$ pair and random combinations of $\pi^-\pi^+\pi^-\pi^+$. We estimate a fraction of 80% for random combinations of $\pi^-\pi^+\pi^-\pi^+$ and 20% for $\rho(770)^0$ plus a $\pi^-\pi^+$ pair. Random combinations of two ρ^0 might be also present, although with a small contribution. The background fractions, as well as its composition, is a source of systematic uncertainty.

We assume the random $\pi^-\pi^+\pi^-\pi^+$ combinations to be uniformly distributed in phase space, whereas for the other background we assume a Breit-Wigner with no form factors and no angular distribution. The overall background distribution is a weighted, incoherent sum of the two components described above. The relative background fractions, b_k, are fixed in the fit.

5. Detector resolution and acceptance correction

The finite momentum resolution causes a smearing of the phase space boundary. It is easier to understand this effect if we consider the case of a three-body decay and the Dalitz plot. In a sample where the three-body masses have only one well defined value, the Dalitz plot boundary is also well defined and unique. But in a sample where we have a distribution of three-body masses, $G(M)$, the Dalitz plot boundary is no longer well defined but, rather, it is a superposition of boundaries, each one defined by its corresponding value of the three-body mass. Dividing the three-body mass distribution into fine bins, one can think of the observed $s_{12} \times s_{23}$ distribution as a superposition of Dalitz plots, each one weighted by $G(M_i)$. The same reasoning applies to four-body decays. We incorporate the effect of the momentum resolution, both in the signal and background probability distribution functions (PDF), by weighting each event by the 4π mass distribution. With this approach, the signal and background PDF depend on the five invariants and on the 4π mass as well.

The acceptance correction is also applied on an event-by-event basis. The acceptance is a function of the five invariants. In the case of the amplitude analysis, the absolute value of the acceptance function is irrelevant, since it implies an overall constant factor multiplying the likelihood. All one really needs to know is the acceptance at a given phase space cell relative to its neighbor cells. We use a five-dimensional matrix for the acceptance correction rather than a continuous function. We used the full FOCUS Monte Carlo simulation (ROGUE) to generate a very large sample of $D^0 \to \pi^-\pi^+\pi^-\pi^+$ events with a constant matrix element.

We applied the same selection criteria to this sample as those used for real data. A mini-MC simulation of the $D^0 \to \pi^-\pi^+\pi^-\pi^+$ was used to generate the phase space distribution. Each of the five axes were divided into bins. Two five-dimensional arrays were filled, one with the events of the full simulation that passed all cuts and the other with the phase space events. The acceptance matrix was formed by dividing the number of ROGUE events in each cell by the number of phase space events in that cell. The acceptance is nearly uniform across the phase space, with a 10-15% decrease close to the edges.

6. Normalization

The maximum likelihood fit technique requires the likelihood function to be normalized. This means one normalization constant for the signal and another for the background probability distribution functions. The normalization constant for the background distribution needs to be calculated just once, since the background amplitudes and the relative fractions are fixed during the fit. The normalization constant for the signal, however, must be computed at each step of the minimization procedure, since it involves the fit parameters.

Although it is not necessary, the amplitudes for each intermediate state are normalized to unity. This is intended to give the magnitudes c_k a direct physical meaning: the decay fraction of each mode is directly proportional to $|c_k|^2$.

The normalization is a crucial step in amplitude analysis. The evaluation of the normalization constants requires a number of phase space integrals. Fortunately this integration can be performed just once, since all input parameters in the amplitudes — mass and width of resonances, form factors parameter — are fixed during the minimization process.

We define $G(m_{4\pi})$ and $b(m_{4\pi})$ as functions representing the 4π mass signal and background distributions, respectively. The function $G(m_{4\pi})$ is a sum of two Gaussians, whereas $b(m_{4\pi})$ is a sum of two exponentials. Both $G(m_{4\pi})$ and $b(m_{4\pi})$ were obtained by the fit to the 4π mass spectrum shown in Fig. 1. If we define ϕ as a point in phase space ($d\phi = ds_{12}ds_{14}ds_{23}ds_{34}ds_{13}$), $\rho(\phi)$ as the phase space density, and $\varepsilon(\phi)$ as the efficiency, and $\bar{A}_k(\phi)$, $\bar{B}_j(\phi)$ the unormalized amplitudes, the normalization integrals are

$$N_k^S = \int dm_{4\pi}\; G(m_{4\pi}) \int d\phi\; \rho(\phi) \left|\bar{A}_k(\phi)\right|^2 \tag{11}$$

and

$$N_j^B = \int dm_{4\pi}\ b(m_{4\pi}) \int d\phi\ \rho(\phi)\bar{B}_j(\phi). \tag{12}$$

The overall signal and background normalization integrals are

$$N_S = \int dm_{4\pi}\ G(m_{4\pi}) \int d\phi\ \rho(\phi)\varepsilon(\phi) \left|\sum c_k A_k(\phi)\right|^2 \tag{13}$$

and

$$N_B = \int dm_{4\pi}\ b(m_{4\pi}) \int d\phi\ \rho(\phi)\varepsilon(\phi) \sum b_j B_j(\phi), \tag{14}$$

with $A_k(\phi) = \bar{A}_k(\phi)/N_k^S$ and $B_j(\phi) = \bar{B}_j(\phi)/N_j^B$.

We performed the phase space integration using the Monte Carlo. The $m_{4\pi}$ interval is divided into bins. For each $m_{4\pi}$ bin a very large sample of MC events, generated with a constant matrix element, is used to compute average value of the integrands. These average values are then multiplied by the phase space volume and weighted by $G(m_{4\pi})/b(m_{4\pi})$.

7. The likelihood function

The overall signal and background amplitudes are corrected on an event-by-event basis for the acceptance, which is nearly constant across the phase space, and for the finite detector resolution, taken into account by multiplying the overall signal distribution by a Gaussian factor, $G(m_{4\pi})$, and the background distribution by an exponential function, $b(m_{4\pi})$. The normalized signal probability distribution is, thus,

$$S_{\rm PDF}(\phi; m_{4\pi}) = \frac{1}{N_S} G(m_{4\pi}) \left|\sum c_k A_k(\phi)\right|^2, \tag{15}$$

and

$$P_S(\phi; m_{4\pi}) = \varepsilon(\phi)\rho(\phi) S_{\rm PDF}(\phi; m_{4\pi}). \tag{16}$$

The normalized background probability distribution is

$$B_{\rm PDF}(\phi; m_{4\pi}) = \frac{1}{N_B} b(m_{4\pi}) \sum b_k B_k(\phi), \tag{17}$$

and

$$P_B(\phi; m_{4\pi}) = \varepsilon(\phi)\rho(\phi)B_{\rm PDF}(\phi; m_{4\pi}). \tag{18}$$

An unbinned maximum likelihood fit was performed, minimizing the quantity $w \equiv -2\log(\mathcal{L})$. The likelihood function, $\mathcal{L}$, is

$$\mathcal{L} = \prod_{\rm events} \left[P_S(\phi^i; m^i_{4\pi}) + P_B(\phi^i; m^i_{4\pi})\right] = \prod_{\rm events} \left[\varepsilon(\phi^i)\rho(\phi^i)(S_{\rm PDF}(\phi^i; m^i_{4\pi}) + B_{\rm PDF}(\phi^i; m^i_{4\pi}))\right] \tag{19}$$

When we take the logarithm of the likelihood we have

$$\log\mathcal{L} = \sum_{\rm events} \log\left[\varepsilon(\phi^i)\rho(\phi^i)\right] + \sum_{\rm events} \log\left[S_{\rm PDF}(\phi^i; m^i_{4\pi}) + B_{\rm PDF}(\phi^i; m^i_{4\pi})\right] \tag{20}$$

In the fit parameter space the term $\sum \log\left[\varepsilon(\phi^i)\rho(\phi^i)\right]$ is a constant and does not affect the position of the minimum. In practice, thus, we minimize the quantity

$$w = -2\left[\sum_{\rm events} \log\left(\frac{1}{N_S}G(m_{4\pi})\left|\sum c_k A_k(\phi^i)\right|^2 + \frac{1}{N_B}b(m_{4\pi})\sum b_k B_k(\phi^i)\right)\right]. \tag{21}$$

The acceptance correction and the phase space density enter only in the overall normalization constants N_S and N_B.

Decay fractions are obtained from the coefficients c_k, determined by the fit, and after integrating the overall signal amplitude over the phase space at $m_{4\pi} = m_{D^0}$,

$$f_k = \frac{\int d\phi \left|c_k A_k(\phi)\right|^2}{\int d\phi \left|\sum_j c_j A_j(\phi)\right|^2} = \frac{\left|c_k\right|^2}{\int d\phi \left|\sum_j c_j A_j(\phi)\right|^2}, \tag{22}$$

since the individual amplitudes $A_k(\phi)$ are normalized to unity. Errors on the fractions include errors on both magnitudes and phases, and are computed using the full covariance matrix.

VI. RESULTS FROM AMPLITUDE ANALYSIS

The technique described in Section V is applied to the events in the hatched area of Fig. 3. The decay $D^0 \to a_1^+\pi^-$, $a_1^+ \to \rho^0\pi^+$ (S-wave) is taken as the reference mode, fixing the phase convention and the relative magnitudes of the other contributions. The results of the

TABLE III: Results from the best fit. The first error is statistical, and the second one is systematic.

mode	magnitude	phase (degrees)	fraction (%)
$a_1^+\pi^-,\ a_1 \to \rho^0\pi^+$ (S-wave)	1. (fixed)	0 (fixed)	$43.3 \pm 2.5 \pm 1.9$
$a_1^+\pi^-,\ a_1 \to \rho^0\pi^+$ (D-wave)	$0.241 \pm 0.033 \pm 0.024$	$82 \pm 5 \pm 4$	$2.5 \pm 0.5 \pm 0.4$
$a_1^+\pi^-,\ a_1 \to \sigma\pi^+$	$0.439 \pm 0.026 \pm 0.021$	$193 \pm 4 \pm 4$	$8.3 \pm 0.7 \pm 0.6$
$a_1^+\pi^-$ (all)	-	-	$60.0 \pm 3.0 \pm 2.4$
$\rho^0\rho^0$ (parallel)	$0.157 \pm 0.027 \pm 0.020$	$120 \pm 7 \pm 8$	$1.1 \pm 0.3 \pm 0.3$
$\rho^0\rho^0$ (perpendicular)	$0.384 \pm 0.020 \pm 0.015$	$163 \pm 3 \pm 3$	$6.4 \pm 0.6 \pm 0.5$
$\rho^0\rho^0$ (longitudinal)	$0.624 \pm 0.023 \pm 0.015$	$357 \pm 3 \pm 3$	$16.8 \pm 1.0 \pm 0.8$
$\rho^0\rho^0$ (all)	-	-	$24.5 \pm 1.3 \pm 1.0$
$f_0(980)\pi^+\pi^-$	$0.233 \pm 0.019 \pm 0.015$	$261 \pm 7 \pm 4$	$2.4 \pm 0.5 \pm 0.4$
$f_2(1270)\pi^+\pi^-$	$0.338 \pm 0.021 \pm 0.016$	$317 \pm 4 \pm 4$	$4.9 \pm 0.6 \pm 0.5$
$\sigma\pi^+\pi^-$	$0.432 \pm 0.027 \pm 0.022$	$254 \pm 4 \pm 5$	$8.2 \pm 0.9 \pm 0.7$
$R\pi^+\pi^-$ (all)	-	-	$20.0 \pm 1.2 \pm 1.0$

best fit to the data are summarized in Table III. The systematic errors are discussed in Section VI.E.

In Fig. 3 the $\pi\pi$ mass projections from data (diamonds with error bars) is plotted with the fit result overlaid (solid histograms). The fit projections are made from a large MC simulated sample, including the signal and background PDF's, defined in Eq. (15) and (17), as well as the reconstruction efficiency and detector resolution. In Fig. 3(a) the $\pi^-\pi^+$ mass is shown. Events in Fig. 3(b) and (c) are the $\pi^-\pi^+$ combinations with highest and lowest mass, respectively. In Fig. 3(d) we show the $\pi^-\pi^-/\pi^+\pi^+$ invariant mass.

The $\pi^+\pi^-\pi^+$ mass spectrum is shown in Fig. 4. This plot has four entries per event. The diamonds with error bars are the data distribution, whereas the solid histogram is the fit projection. Note that this distribution does not reflect the pure $a_1(1260)$ line shape, for, in addition to the Bose-symmetrization, there are contributions from the other modes.

A further comparison between the fit result and the data can be made with the pion momentum distribution, computed in the D rest frame. Recall that we do not distinguish between D^0 and $\overline{D}^0$, and that there is no particle ordering according to its momentum. This means that all pions must have the same momentum distribution and that we can add

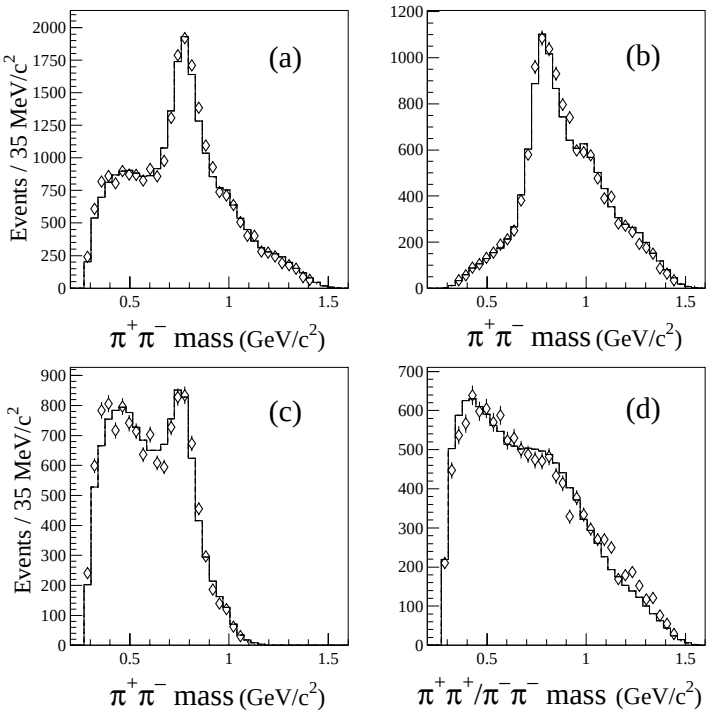

FIG. 3: Comparison between data and the result of the best fit. In (a) all four $\pi^-\pi^+$ combinations are added. Entries from plot (a) are split into combinations with highest and lowest $\pi^-\pi^+$ mass: in (b) we show the $\pi^-\pi^+$ combinations with highest mass, whereas in (c) we show the $\pi^-\pi^+$ combinations with lowest mass; finally, in (d) we show the $\pi^-\pi^-/\pi^+\pi^+$ mass distribution. In all plots the solid histogram is a projection of the fit.

them into a single plot. The pion momentum distribution is shown in Fig. (5), where the diamonds represent the data points, and the solid histogram is a MC simulation.

We can also compute the acoplanarity angle. In the $D \to RR$ decay this is the angle, measured in the D rest frame, between the planes defined by the decay particles of each of the resonances. Note that in the $D^0 \to \pi^-\pi^+\pi^-\pi^+$ decay the $\rho^0\rho^0$ mode accounts for only one fourth of the decay rate, so the distribution of the acoplanarity angle no longer carries the information on the polarization state of the two vector mesons. The distribution cosine of the acoplanarity angle is shown in Fig. 6. Once more, the diamonds represent the data points, and the solid histogram is a projection of the fit.

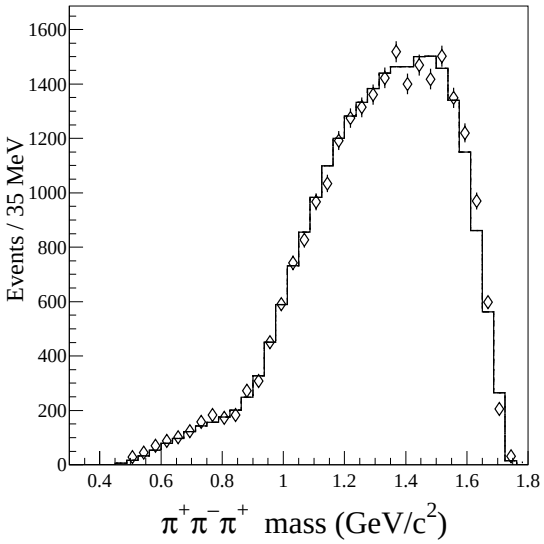

FIG. 4: The $\pi^+\pi^-\pi^+/\pi^-\pi^+\pi^-$ mass spectrum. A projection of the fit (solid histogram) is overlaid with the data points (diamonds with error bars).

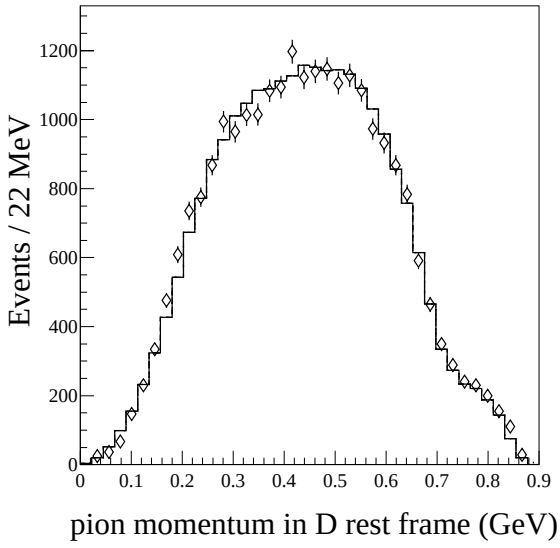

FIG. 5: The pion momentum distribution in the D rest frame (four entries per event). The momentum distribution for all pions should be the same, so in this plot there are four entries per event. A projection of the fit (solid histogram) is overlaid with the data points (diamonds with error bars).

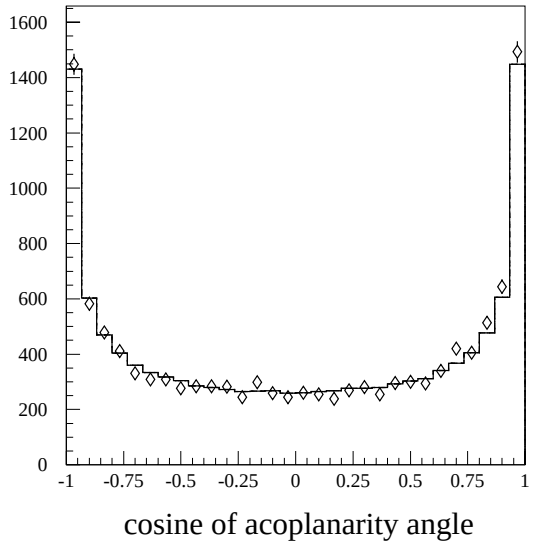

FIG. 6: The cosine of the acoplanarity angle distribution. The contribution of the $D^0 \to \rho^0\rho^0$ is only 25%, so the original polarization of the two vector states is diluted.

A. Goodness-of-fit

The $\pi^+\pi^-$ and the $\pi^+\pi^-\pi^+$ mass spectra, as well as the pion momentum and the cosine of the acoplanarity angle distribution, are reasonably well represented by our model. These are, however, inclusive distributions, indicating that the model represents the general features of the data. Any quantitative statements about the fit quality should be made by inspecting the five-dimensional phase space.

The goodness-of-fit is assessed using a χ^2-like test. The phase space is divided in equally-sized, five-dimensional cells. For each of these, the expected number of events, $n_{\rm fit}$, is obtained by the MC simulation described above, after scaling the MC sample to the number of events in the data sample. For each cell with a minimum expected occupancy of 5 events, a χ^2 is computed comparing the predicted population to the observed number of events, $(n_{\rm obs} - n_{\rm fit})/\sigma$, where $\sigma = \sqrt{n_{\rm obs}}$. The total χ^2 is formed by summing over all cells with minimum occupancy. The number of degrees of freedom is the number of cells with minimum occupancy minus the number of free parameters in the fit. The baseline model has 9 amplitudes, with 16 free parameters. There are 166 bins with at least the minimum occupancy, so the number of degrees of freedom is 150. These bins include 97% of the data.

The total χ^2 is 348.0, which corresponds to a confidence level (CL) of 10^{-17}. We conclude from the χ^2 test that the baseline model does not provide an accurate description of the data in the five-dimensional phase space.

We have looked at the distribution of the χ^2 throughout the phase space. That might reveal the need of a missing resonant amplitude, or problems with the representation of the existing amplitudes. We found that there are 33 bins with $\chi^2 > 6$, containing approximately 15% of the data events. The bins that are responsible for the poor confidence level of the fit are evenly distributed throughout the phase space, instead of being concentrated in specific regions. In general, these 33 bins are surrounded by bins having a good χ^2.

Addition of further amplitudes of the type $D \to RR$ do not improve the fit quality. The inclusion of an uniform nonresonant term gives rise to large interference with the $\sigma\pi^+\pi^-$ mode without improving the likelihood. A fit using an alternative model, in which the $D \to \sigma\pi^+\pi^-$ mode is replaced by a uniform nonresonant amplitude, is worse than our best fit by more than 200 units of $w = -2\log\mathcal{L}$. No improvement is obtained when other amplitudes of the type $D \to R\pi^+\pi^-$ are added. The contribution from $D^0 \to \rho^0\pi^+\pi^-$ is negligible. This is also the case for amplitudes with higher mass states, like the $\rho(1450)^0\pi^+\pi^-$ and the $f_0(1370)\pi^+\pi^-$.

It is very unlikely that the poor CL is caused by problems with the representation of the signal amplitudes cause of. The dominant resonance is the $\rho(770)^0$, which has a very well determined line shape. As we will discuss on Section VI.E, the uncertainty in the line shape of the S-wave components does not have a large impact on the fit result. The other ingredients of the signal amplitudes are the standard angular distributions and the well known, widely used Blatt-Weisskopf form factors, depending on one single parameter whose value does not significantly affect the fit result.

The isobar model is a very standard tool, and has been successfully used for several decades. Almost all Dalitz plot analyses of heavy flavor decays were performed by representing the signal distribution as a coherent sum of resonant amplitudes with constant coefficients. The isobar model has also been successful in describing four-body decays in the past [33, 34] (although no CL was quoted in these analyses) and recently [35, 36], but in all cases the data samples have limited statistics. This analysis is the first attempt to use the isobar model for an amplitude analysis of a four-body decay with moderately high statistics. The underlying picture of the isobar model may be too simplistic, signaling other types of

effects should be taken into account.

B. General features of the best solution

The dominant contribution to the $D^0 \to \pi^-\pi^+\pi^-\pi^+$ decay comes from the $D^0 \to a_1(1260)^+\pi^-$ mode, accounting for 60% of the decay rate. The second most dominant contribution is the $D^0 \to \rho(770)^0\rho(770)^0$ mode, with a decay fraction of 25%. Modes of the type $D \to R\pi^+\pi^-$ correspond to 20% of the decay rate.

The large value of the $D^0 \to a_1(1260)^+\pi^-$ decay fraction supports the picture of an external W-radiation amplitude, with the virtual W coupling to the $a_1(1260)$, as the dominant mechanism for the $\pi^-\pi^+\pi^-\pi^+$ final state. The same dominance has also been observed in other four-body decays, such as $D^0 \to K^-\pi^+\pi^-\pi^+$ and $D^+ \to \overline{K}^0\pi^+\pi^-\pi^+$ [33, 34]. The same picture can be drawn in the case of three-body decays with the W coupling to the $\rho(770)^+$, such as $D^0 \to K^-\pi^+\pi^0$ [37] or $D^+ \to \overline{K}^0\pi^+\pi^0$ [38], where the contribution from $D \to K\rho$ exceeds 50%. This pattern is similar to the well known vector-dominance in electromagnetic interactions. It can be understood as a manifestation of the V-A nature of the weak interaction.

The relatively large contribution (25%) of the $D \to \rho^0\rho^0$ ($D \to V_1^0V_2^0$) decay has also been seen in other final states, such as $D^0 \to K^-\pi^+\pi^-\pi^+$, where the mode $D^0 \to \overline{K}^{*0}\rho^0$ accounts for 17% of the decay rate, according to [33] or over 40%, according to [34]. In the case of the final state $D^0 \to K^-K^+\pi^-\pi^+$ [36], the contribution of the modes $D^0 \to \rho^0\phi$ and $D^0 \to \overline{K}^{*0}K^{*0}$ amounts to more than 30%. In all cases the dominant $D \to V_1^0V_2^0$ amplitude is the internal W-radiation, which is expected to be suppressed with respect to the external W-radiation amplitude.

The remainder of the decay rate is due to three-body nonresonant modes $D \to R\pi^+\pi^-$. Like the $D \to \rho^0\rho^0$ decay, the internal W-radiation should be the dominant amplitude. For any possible meson R there are several ways to form a $R\pi^+\pi^-$ state with $J = 0$, combining the orbital angular momentum between the two pions from the nonresonant $\pi^+\pi^-$ system, the orbital angular momentum between this system and the resonance R, and the spin of the resonance. Consequently, for any possible resonance R we can assign different spin amplitudes. We tried all possible assignments for the $\rho(770)^0\pi^+\pi^-$ and for the $\rho(1450)^0\pi^+\pi^-$ spin amplitudes, but none yielded a significant contribution. It is interesting to note that

the only $D \to R\pi^+\pi^-$ modes with a significant contribution are $\sigma\pi^+\pi^-$, $f_0(980)\pi^+\pi^-$ and $f_2(1270)\pi^+\pi^-$, with the nonresonant $\pi^+\pi^-$ pair being in a pseudoscalar state. The $\pi^+\pi^-$ pair and the resonance must then be in a state of even relative orbital angular momentum, and the resulting spin amplitudes coincide with the ones from three-body D decays [19].

C. $a_1(1260)$ results

As we mentioned before, the study of the $a_1(1260)$ is one of the main purposes of this analysis. The a_1 line shape is connected to the resonant substructure through Eq. (9). The data seem to require, in addition to the dominant $a_1^+ \to \rho(770)^0\pi^+$ amplitude, an S-wave component $a_1^+ \to \sigma\pi^+$, as in the case of CLEO [31] and E852 [39]. A fit without the $\sigma\pi^+$ mode increases the quantity $w = -2\log\mathcal{L}$ by more than 200. We tried other modes, such as the $a_1^+ \to f_0(980)\pi^+$, $a_1^+ \to \rho(1450)^0\pi^+$ and $a_1^+ \to f_0(1370)\pi^+$, but their contribution is negligible. We have also made a fit with the $a_1^+ \to f_0(980)\pi^+$ and $a_1^+ \to f_2(1270)\pi^+$ amplitudes replacing the $f_0(980)\pi^+\pi^-$ and $f_2(1270)\pi^+\pi^-$. This fit is worse by more than 100 units of $w = -2\log\mathcal{L}$.

We found that the three channels for the a_1 resonant substructure are necessary and sufficient for a description of the data. Our model for the a_1 substructure is the same as that of E852, but it is in contrast with the CLEO analysis of $\tau^- \to \nu_\tau\pi^+\pi^0\pi^0$ [31]. The CLEO fit to the $\pi^+\pi^0\pi^0$ line shape required seven different contributions. However, the three analyses agree on the general picture of the a_1 substructure, according to which the dominant contribution comes from the S-wave $\rho(770)^0\pi$, (over 60% of the a_1 decay rate), followed by the $\sigma\pi$ ($\sim$15%) and with a small D-wave $\rho(770)^0\pi$ component.

From the results of the a_1 resonant substructure we can measure the ratio between the D- and S-wave $\rho^0\pi^+$ amplitudes. In the flux-tube-breaking model [40] this ratio is given by

$$\frac{A(a_1 \to (\rho\pi)_D)}{A(a_1 \to (\rho\pi)_S)} = \frac{-D}{\sqrt{32}S}, \tag{23}$$

where D and S are the D- and S-wave amplitudes. Using this definition we measure

$$\frac{A(a_1 \to (\rho\pi)_D)}{A(a_1 \to (\rho\pi)_S)} = -0.043 \pm 0.009 \pm 0.005, \tag{24}$$

where the statistical uncertainty is obtained from the full covariance matrix.

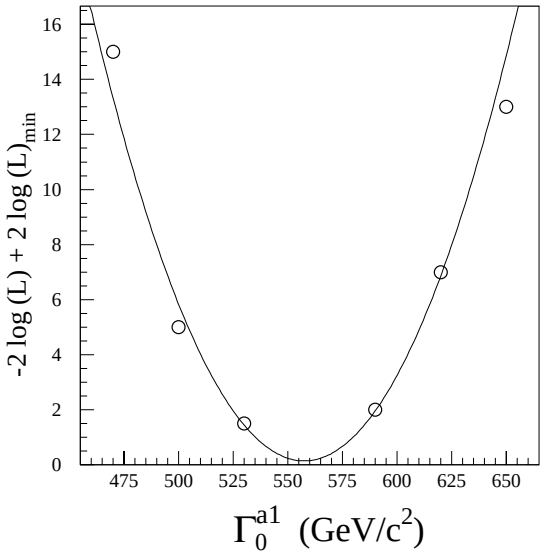

FIG. 7: The difference $-2\log\mathcal{L} + 2\log\mathcal{L}_{\max}$ as a function of the $\Gamma_0^{a_1}$ parameter, for $\sqrt{s_0^{a_1}} = 1240$ MeV/c^2.

The $a_1(1260)$ line shape was determined by the iterative procedure described above. We scanned over the values $s_0^{a_1}$ and $\Gamma_0^{a_1}$ in order to find the combination of values that optimizes the fit result. The resonant substructure remained stable during this scanning procedure; that is, the values of c_i varied less than 10%. We found that there is some correlation between $s_0^{a_1}$, $\Gamma_0^{a_1}$ and the cefficients c_i. Fits of nearly equivalent quality can be obtained using combinations of these parameters along the diagonal of a rectangle, in the $\sqrt{s_0^{a_1}} \times \Gamma_0^{a_1}$ plane, with sides $1230 < \sqrt{s_0^{a_1}} < 1270$ MeV/c^2 and $520 < \Gamma_0^{a_1} < 680$ MeV/c^2. The optimum values are $\sqrt{s_0^{a_1}} = 1240$ MeV/c^2 and $\Gamma_0^{a_1} = 560$ MeV/c^2.

These values differ significantly from CLEO result: $\sqrt{s_0^{a_1}} = (1331 \pm 10)$ MeV/c^2 and $\Gamma_0^{a_1} = (814 \pm 38)$ MeV/c^2. The CLEO values, however, depend strongly on their form factor parameter r. When the value of this parameter is set to $r = 1.2$ GeV^{-1} in the CLEO analysis, their values of $\sqrt{s_0^{a_1}}$ and $\Gamma_0^{a_1}$ are in very good agreement with the result of this analysis. Our result is in good agreement with the model of Kühn and Santamaria [41] ($\sqrt{s_0^{a_1}} = (1262 \pm 11)$ MeV/c^2 and $\Gamma_0^{a_1} = (621 \pm 66)$ MeV/c^2) and a bit higher than the values from Isgur *et al.* ($\sqrt{s_0^{a_1}} = (1210 \pm 7)$ MeV/c^2 and $\Gamma_0^{a_1} = (457 \pm 23)$ MeV/c^2) [40]. Both models consider only the $\rho\pi$ mode for the a_1 resonant substructure.

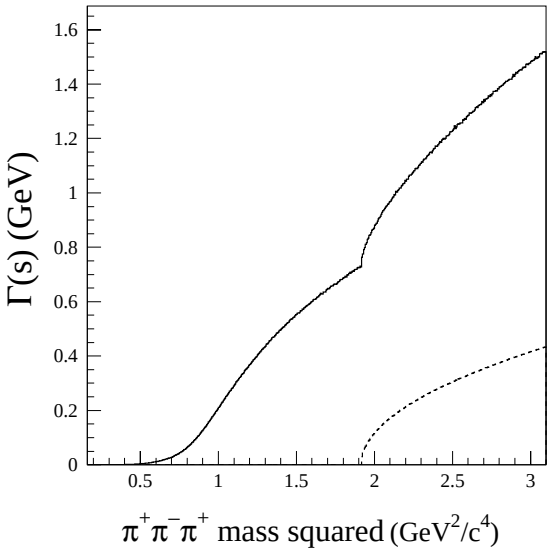

FIG. 8: The s-dependent a_1 width, $\Gamma^{a_1}_{\rm tot}(s)$, plotted as a function of the $\pi^+\pi^-\pi^+$ mass squared, s. The dashed line represents the contribution from $a_1 \to K^*K$.

D. $D^0 \to \rho^0\rho^0$ results

The amplitude for the $D \to \rho^0\rho^0$ decay is written in the helicity formalism. The most general amplitude $D \to V_1(\lambda_1)V_2(\lambda_2)$ is a sum of three independent components, corresponding to the linear polarization states of the vector mesons. The D^0 is an initial state with $J = 0$, so the vector mesons helicities λ_1 and λ_2 must be equal, $\lambda_1 = \lambda_2 = \lambda = -1, 0, +1$. The three independent helicity amplitudes, corresponding to each of the possible helicity states are H_-, H_0, and H_+. Alternatively, one can decompose the $D \to V_1V_2$ decay amplitude in the so-called transversity basis [42], with amplitudes given by $A_0 = H_0$, $A_{\|} = (H_+ + H_-)/\sqrt{2}$ and $A_\perp = (H_+ - H_-)/\sqrt{2}$. This basis represents states in which the vector mesons are longitudinally polarized (A_0), or transversely polarized ($A_{\|}$, $A_\perp$). The transversity basis states are parity eigenstates.

In the D rest frame the two vector mesons are back-to-back. After a boost along the line-of-flight to the V_1 rest frame, we define the helicity angle θ_1 as the angle between the π^- and the direction of the boost, measured counterclockwise. The helicity angle θ_2 is defined in a similar way. With these definitions and the acoplanarity angle, χ, defined as the angle between the V_1, V_2 decay planes measured in the D frame, one can write the $D \to V_1V_2$

decay amplitude as

$$\mathcal{A}(D \to \rho\rho) \propto A_0 \cos\theta_1 \cos\theta_2 + \frac{A_\parallel}{\sqrt{2}} \sin\theta_1 \sin\theta_2 \cos\chi - i\frac{A_\perp}{\sqrt{2}} \sin\theta_1 \sin\theta_2 \sin\chi. \quad (25)$$

In the above equation the amplitudes A_0, $A_\parallel$, and $A_\perp$ are of the form $A_i = a_i e^{i\delta_i} f(m^2_{\pi\pi})$, where a_i and δ_i are real constants and $f(m^2_{\pi\pi})$ has all the energy dependent terms: Breit-Wigner functions, form factors, and the energy dependent part of the angular distribution.

The longitudinal polarization is defined as the ratio of the longitudinal to the total decay rate,

$$P_L = \frac{|A_0|^2}{|A_0|^2 + |A_\parallel|^2 + |A_\perp|^2}. \quad (26)$$

Using the values obtained by the fit (Table III) we measured $P_L = (71 \pm 4 \pm 2)\%$.

Our value is in agreement with the BABAR result from $B^0 \to \rho^0\rho^0$ [12], $P_L = (87 \pm 13 \pm 4)\%$, but is somewhat different from the polarization measured in $B^0 \to \rho^+\rho^-$ ($P_L = (99 \pm 3 \pm 4)\%$) [10] and in $B^\pm \to \rho^\pm\rho^0$ ($P_L = (95 \pm 11 \pm 2)\%$ [9] and $P_L = (90.5 \pm 4.2 \pm 2.5)\%$) [11].

The polarization measured in B decays is in agreement with theoretical expectations [43], which are based on the assumption that the transition amplitude for the $B \to \rho\rho$ can be written as a product of two independent hadronic currents. The factorization hypothesis may be a good approximation for B meson decays, due to the large value of its mass, but fails to describe hadronic decays of D mesons. That could explain the observed difference in the values of the longitudinal polarization fraction from D and B decays.

E. Systematic uncertainties

The representation of the structures present in $\pi^-\pi^+\pi^-\pi^+$ is a major source of systematic uncertainty. The problem starts with the choice of a set of amplitudes to describe the data. Furthermore, our model depends on some input parameters, which are fixed during the fit: the parameter r_R for the form factors; the a_1 parameters $s_0^{a_1}$, $\Gamma_0^{a_1}$ and g_{K^*K}; the relative amount of the backgrounds. In addition, there are the parameters defining the σ and the $f_0(980)$ line shape: m_0^σ and Γ_0^σ, and g_π, g_K, and $m_0^{f_0}$. We should also mention that there is some freedom in the choice of the angular distributions.

We investigated the effect of the uncertainty on the input parameters of our model on the fractions and phases for the various intermediate channels. For this purpose, the data was fit with variations of our baseline model. We varied the value of r_R from 1 to 5 GeV^{-1}. We have also fit the data using different sets of a_1 parameters, $s_0^{a_1}$, $\Gamma_0^{a_1}$ and g_{K^*K}. For the σ and $f_0(980)$ line shapes we used the BES parameterization [44, 45].

In addition, we varied the background parameterization: the relative amount of background, the background composition, adding a possible contribution from uncorrelated $\rho^0\rho^0$ events, and the relative fractions of the backgrounds, changing the fraction of $\rho^0\pi^+\pi^-$ from 0 to 50%.

A very small change of the values of the fit parameters, compared to their central values, is observed when we vary the r_R parameter, the background parameterization and the $f_0(980)$ line shape. The systematic errors are largely dominated by the uncertainty in the a_1 parameters and on the σ line shape, in this order. The total systematic errors are taken as the root mean square of fit variations. These are propagated to fractions, the longitudinal polarization measurement, and the D/S ratio. The systematic errors are quoted in Table III.

VII. CONCLUSIONS

In this paper we presented a new measurement of the relative branching ratio $\Gamma(D^0 \to \pi^+\pi^-\pi^+\pi^-)/\Gamma(D^0 \to K^-\pi^+\pi^-\pi^+) = 0.0914 \pm 0.0018 \pm 0.0022$, based on a very clean sample of 6360 ± 115 events. Our value is compatible with the recent CLEO-c result [20], which has a sample of comparable size, but with a higher background level.

A full, coherent amplitude analysis of the $D^0 \to \pi^-\pi^+\pi^-\pi^+$ decay was made for the first time. The isobar model with nine resonant amplitudes provides a description of the general features of the data. In our model there are contributions of three types. The dominant contribution comes from the decay $D^0 \to a_1(1260)^+\pi^-$, accounting for 60% of the total decay rate. This is followed the decay $D^0 \to \rho(770)^0\rho(770)^0$, whose relative fraction amounts to 25%, and by the three-body nonresonant decays $D^0 \to \sigma\pi^+\pi^-$, $D^0 \to f_0(980)\pi^+\pi^-$ and $D^0 \to f_2(1270)\pi^+\pi^-$, with a combined fraction of 20%.

The $D^0 \to \pi^-\pi^+\pi^-\pi^+$ decay is a very suitable tool for investigation of the $a_1(1260)$ meson. A good description of this state is achieved assuming a simple resonant substructure, with

only three contributions: a dominant $a_1^+ \to \rho(770)^0\pi^+$ S-wave, a small $a_1^+ \to \rho(770)^0\pi^+$ D-wave, and the $a_1^+ \to \sigma\pi^+$. In the framework of the flux-tube-breaking model, we measure the $a_1^+ \to \rho(770)^0\pi^+$ D/S ratio to be $R = -0.043 \pm 0.009 \pm 0.005$.

The line shape of the $a_1(1260)$ is also an output of the amplitude analysis. The best description of our data is achieved with the $a_1(1260)$ Breit-Wigner parameters, $\sqrt{s_0^{a_1}}$ and $\Gamma_0^{a_1}$, in the range $1230 < \sqrt{s_0^{a_1}} < 1270$ MeV/c^2 and $520 < \Gamma_0^{a_1} < 680$ MeV/c^2, with optimum values at $\sqrt{s_0^{a_1}} = 1240$ MeV/c^2 and $\Gamma_0^{a_1} = 560$ MeV/c^2.

The $D^0 \to \pi^-\pi^+\pi^-\pi^+$ decay has an important $\rho^0\rho^0$ component. The helicity formalism is used to to describe the angular distribution of the four pions from this mode. Using the transversity basis states and a full amplitude analysis, we measure the ratio of the longitudinal polarization to the total $D \to \rho^0\rho^0$ rate to be $P_L = (71 \pm 4 \pm 2)\%$.

The fit quality, from an inspection of the five-dimensional phase space, is poor and it is not improved by changing the representation of individual signal amplitudes or by adding other amplitudes to the baseline model. We conclude that in the case of $D^0 \to \pi^-\pi^+\pi^-\pi^+$ the failure of the isobar model in providing an accurate description of our data suggests that other type of effects should be taken into account. Possible candidates are the Bose-Einstein correlations or a non-uniform nonresonant amplitude. The most crucial missing ingredient may be the energy dependent final state interactions. Unfortunately this is a very difficult problem, even for three-body decays. To our knowledge, there are no calculations of the effects of FSI in four-body decays. This problem, however, must be addressed in order to explore the full potential of the hadronic decays of heavy flavor and the amplitude analysis technique.

Acknowledgments

We wish to acknowledge the assistance of the staffs of Fermi National Accelerator Laboratory, the INFN of Italy, and the physics departments of the collaborating institutions. This research was supported in part by the U. S. National Science Foundation, the U. S. Department of Energy, the Italian Istituto Nazionale di Fisica Nucleare and Ministero della Istruzione Università e Ricerca, the Brazilian Conselho Nacional de Desenvolvimento Científico e Tecnológico, CONACyT-México, and the Korea Research Foundation of the Korean Ministry of Education.

APPENDIX A: ANGULAR DISTRIBUTIONS

The angular distributions of the final state particles result from angular momentum conservation throughout the whole decay chain. These distributions depend on both the spin of the intermediate resonances and on the orbital angular momentum at each vertex. In the case of sequential decays, like the $D \to a_1^+\pi^-$, $a_1^+ \to \rho^0\pi^+$, $\rho^0 \to \pi^+\pi^-$ chain, parity conservation is also a constraint on the a_1 decay and all its subsequent decay products.

Amplitudes describing angular distributions, hereafter called spin amplitudes for short, are, in general defined using the relativistic tensor formalism [25, 26]. This formalism explores the connection between the only available observables — the momenta of the final state particles — and the spin/orbital angular momentum dynamics. Polarization vectors, representing the spin/orbital angular momentum involved at each vertex, as well as all relevant 4-momenta, are written in terms of these final state momenta. Covariance, invariance under rotations and parity conservation, whenever applicable, restricts the many possible combinations between 4-momenta and polarization vectors.

The relativistic tensor formalism was used in this analysis to describe all intermediate channels, except for the $D^0 \to \rho^0\rho^0$, for which we used the helicity formalism.

1. $D \to a_1\pi$

In our model for the a_1 resonant substructure there are three amplitudes: $a_1^+ \to \rho^0\pi^+$, with the ρ^0 and the π^+ in relative S- and D-wave; and the $a_1^+ \to \sigma\pi^+$. We denote the a_1 and ρ^0 polarization 4-vectors with helicity λ by $\varepsilon_\mu(\lambda)$ and $e_\mu(\lambda)$, respectively.

We form Lorentz scalars at each step of the decay sequence by contracting these polarization vectors with the appropriate 4-momenta. In a step where the resonance appears as a decay product, the complex conjugate of its polarization 4-vector is used. If the a_1 is formed by particles 1, 2 and 3, then the amplitude for the $D^0 \to a_1^+\pi_4^-$ is

$$\langle a_1\pi_4\,|A|\,D\rangle \propto \varepsilon^*_\mu(\lambda)p_4^\mu. \tag{A1}$$

The amplitude for the $a_1^+ \to \rho^0\pi^+$ ($\rho^0\pi^+$ in S-wave) decay is

$$\langle \rho\pi\,|A|\,a_1\rangle \propto \varepsilon_\nu(\lambda)e^{*\nu}(\lambda'), \tag{A2}$$

and ($\rho^0\pi^+$ in D-wave)

$$\langle \rho\pi \,|A|\, a_1 \rangle \propto \varepsilon_\nu(\lambda) Q^\nu e^*_\sigma(\lambda') p^\sigma_{a_1}, \tag{A3}$$

with $Q = p_\rho - p_3$, p_ρ, $p_\sigma = p_1 + p_2$ and $p_{a_1} = p_1 + p_2 + p_3$

The amplitude for the ρ^0 decay is

$$\langle \pi\pi \,|A|\, \rho \rangle \propto e_\alpha(\lambda') q^\alpha, \tag{A4}$$

with $q = p_1 - p_2$. Finally, the amplitude for the $a_1^+ \to \sigma\pi^+$ is

$$\langle \sigma\pi \,|A|\, a_1 \rangle \propto \varepsilon_\nu(\lambda) Q^\nu. \tag{A5}$$

We then combine the amplitudes for each step and must sum over the a_1 and ρ^0 polarizations, since none of these states is observed directly. The sum over polarizations is simplified by using the completeness relation [26]

$$\sum_\lambda = \varepsilon^*_\mu(\lambda)\varepsilon_\nu(\lambda) = -g_{\mu\nu} + p_\mu p_\nu / p^2. \tag{A6}$$

After summing over the unobserved polarizations, the spin amplitude for $D^0 \to a_1^+\pi^-_4$, $a_1^+ \to \rho^0\pi^+$ S-wave, $\rho^0 \to \pi^+\pi^-$ is

$$\mathcal{M} = p_4^\mu \left(-g_{\mu\nu} + \frac{p^{a_1}_\mu p^{a_1}_\nu}{p^2_{a_1}} \right) \left(g^{\nu\sigma} - \frac{p^\nu_\rho p^\sigma_\rho}{p^2_\rho} \right) q_\sigma. \tag{A7}$$

For the $a_1^+ \to \rho^0\pi^+$ D-wave the spin amplitude reads

$$\mathcal{M} = p_4^\mu \left(-g_{\mu\nu} + \frac{p^{a_1}_\mu p^{a_1}_\nu}{p^2_{a_1}} \right) Q_\nu p^\sigma_{a_1} \left(-g_{\sigma\alpha} + \frac{p^\rho_\sigma p^\rho_\alpha}{p^2_\rho} \right) q^\alpha. \tag{A8}$$

Finally, the spin amplitude for the $a_1^+ \to \sigma\pi^+$ is

$$\mathcal{M} = p_4^\mu \left(-g_{\mu\nu} + \frac{p^{a_1}_\mu p^{a_1}_\nu}{p^2_{a_1}} \right) Q^\nu. \tag{A9}$$

2. $D \to \rho^0\rho^0$

The spin amplitudes for the $D \to \rho^0\rho^0$ decay are written in the helicity formalism. This decay is of the type $P \to V_1(\lambda_1)V_2(\lambda_2)$, where λ_1, λ_2 are the vector meson helicities. Given

that the initial state has $J = M = 0$, the constraint $|\lambda_1 - \lambda_2| \leq M$ implies that $\lambda_1 = \lambda_2 = \lambda$. The only allowed values for the vector meson helicity are $\lambda = -1$, 0, and $+1$. The helicity-basis states $|JM, \lambda\rangle$ are $|00, -1\rangle$, $|00, 0\rangle$ and $|00, +1\rangle$.

For each helicity state there is one independent amplitude. These amplitudes are functions of the helicity angles, defined in each resonance rest frame, and of the angle formed by the vector mesons decay planes (acoplanarity angle), measured in the D rest frame. We define the z axis along the line of flight of the vector mesons in the D rest frame. With the notation $\rho_1^0 \to \pi_1^- \pi_2^+$ and $\rho_2^0 \to \pi_3^- \pi_4^+$, the helicity angles θ_1 and θ_2 are defined as the angle between π_1 and the z axis, in the ρ_1^0 rest frame, and the angle between π_3 and the z axis, in the ρ_2^0 rest frame.

Now with all momenta measured in the D frame, the orientations of the decay planes are $\hat{n}_1 = \vec{p}(\pi_2^+) \times \vec{p}(\pi_1^-)$ and $\hat{n}_2 = \vec{p}(\pi_4^+) \times \vec{p}(\pi_3^-)$. The acoplanarity angle is $\chi = \hat{n}_1 \cdot \hat{n}_2$.

With the above definitions of θ_1, θ_2 and χ, the general form of the helicity amplitudes is

$$A_\lambda = e^{i\lambda\chi} d^1_{\lambda,0}(\theta_1) d^1_{\lambda,0}(\theta_2). \tag{A10}$$

With the appropriate d functions we have

$$A_{-1} = \frac{1}{2} e^{-i\chi} \sin\theta_1 \sin\theta_2, \tag{A11}$$

$$A_0 = \cos\theta_1 \cos\theta_2, \tag{A12}$$

$$A_{+1} = \frac{1}{2} e^{i\chi} \sin\theta_1 \sin\theta_2. \tag{A13}$$

The helicity-basis states are not parity eigenstates. One can construct a new basis with definite parity,

$$|f_\parallel> = \frac{|00,1\rangle \ + \ |00,-1\rangle}{\sqrt{2}}, \tag{A14}$$

$$|f_\perp> = \frac{|00,1\rangle \ - \ |00,-1\rangle}{\sqrt{2}}, \tag{A15}$$

$$|f_L> = |00,0\rangle. \tag{A16}$$

This is known as the transversity basis [42]. The corresponding amplitudes are

$$A_{\parallel} = \frac{A_{+1} \; + \; A_{-1}}{\sqrt{2}} = \frac{1}{\sqrt{2}} \cos\chi \sin\theta_1 \sin\theta_2, \tag{A17}$$

$$A_{\perp} = \frac{A_{+1} \; - \; A_{-1}}{\sqrt{2}} = \frac{i}{\sqrt{2}} \sin\chi \sin\theta_1 \sin\theta_2, \tag{A18}$$

$$A_L = A_0 = \cos\theta_1 \cos\theta_2. \tag{A19}$$

The above amplitudes are expressed in terms of non-covariant quantities, defined in different reference frames. Covariance is recovered by multiplying the helicity amplitudes by an energy dependent term, which accounts for the boosts from each resonance frame to the D frame. Each of the above amplitudes is then multiplied by

$$A_\lambda \to A_\lambda \times \sqrt{\frac{\Gamma(s)\sqrt{s}}{p^*(s)}}, \tag{A20}$$

where s is the two-pion invariant mass, $p^*(s)$ is the break-up momentum and $\Gamma(s)$ is

$$\Gamma(s) = \Gamma_0 \frac{\sqrt{s_0}}{\sqrt{s}} \left(\frac{p^*(s)}{p^*(s_0)} \right)^3 \frac{1 + (r_R p^*(s_0))^2}{1 + (r_R p^*(s))^2}. \tag{A21}$$

These are the formulae used for the $D \to \rho^0\rho^0$ spin amplitudes.

[1] E.M. Aitala *et al.* (E791 Collaboration), Phys. Rev. Lett. **86**, 770 (2002).

[2] J.M. Link *et al.* (FOCUS Collaboration), Phys. Lett. B **585** 200 (2004).

[3] E.M. Aitala *et al.* (E791 Collaboration), Phys. Rev. D **73**, 032004 (2006).

[4] H. Muramatsu *et al.* (CLEO Collaboration), Phys. Rev. Lett. **89** 251802 (2002).

[5] J.M. Link *et al.* (FOCUS Collaboration), hep-ex/0612032.

[6] S. Pislak *et al.* (E685 Collaboration) Phys. Rev. Lett. **87** 221801 (2001).

[7] B. Hyams *et al.*, Nucl. Phys. B **64**, 134 (1973).

[8] D. Aston *et al.* (LASS Collaboration), Nucl. Phys. B **296**, 493 (1988).

[9] K.Abe *et al.* (Belle Collaboration), Phys. Rev. Lett. **91** 221801 (2003).

[10] B. Aubert *et al.* (BABAR Collaboration), Phys. Rev. Lett. **93** 231801 (2004).

[11] B. Aubert *et al.* (BABAR Collaboration), hep-ex/0607092.

[12] B. Aubert *et al.* (BABAR Collaboration), hep-ex/0612021.

[13] B. Aubert *et al.* (BABAR Collaboration), Phys. Rev. Lett. **97** 051802 (2006).

[14] K.Abe *et al.* (Belle Collaboration), hep-ex/0507096.

[15] P.L. Frabetti *et al.* (E687 Collaboration), Nucl. Instrum. Meth. A **320** 519 (1992)

[16] P.L. Frabetti *et al.* (E687 Collaboration), Nucl. Instrum. Meth. A **329** 62 (1993).

[17] J.M. Link *et al.* (FOCUS Collaboration), Nucl. Instrum. Meth. A **516** 364 (2004).

[18] J.M. Link *et al.* (FOCUS Collaboration), Nucl. Instrum. Meth. A **484** 270 (2002).

[19] W.-M. Yao *et al.* (Particle Data Group), J. Phys. G **33** 1 (2006).

[20] P. Rubin *et al.*(CLEO Collaboration), Phys. Rev. Lett. **96** 081802 (2006).

[21] M. Abiklim *et al.* (BES Collaboration), Phys. Lett. B **622** 6 (2005).

[22] P.L. Frabetti *et al.* (E687 Collaboration), Phys. Lett. B **354** 486 (1995).

[23] I. Bediaga, C. Gobel and R. Mendez-Galain, Phys. Rev. D **56**, 4268 (19797).

[24] J.M. Blatt and V.F. Weisskopf, *Theoretical Nuclear Physics* (Wiley, New York, 1952), p. 361.

[25] V. Filippini, A. Fontana and A. Rotondi, Phys. Rev. D **51**, 2247 (1995).

[26] S.U. Chung Phys. Rev. D **48**, 1225 (1993).

[27] S. Gardner and Ulf-G. Meiszner, Phys. Rev. D **65** 094004 (2002).

[28] A. Abele *et al.* (Crystal Barrel Collaboration), Phys. Lett. B **469** 270 (1999).

[29] A. Abele *et al.* (Crystal Barrel Collaboration), Phys. Lett. B **411** 354 (1997).

[30] S.M. Flatté, Phys. Lett. B **63** 228 (1976).

[31] D.M. Asner *et al.*(CLEO Collaboration), Phys. Rev. D **61**, 012002 (1999).

[32] A. Drustkoy *et al.* (Belle Collaboration), Phys. Lett. B **542** 171 (2002).

[33] D. Coffman *et al.* (Mark III Collaboration), Phys. Rev. D **45**, 2196 (1992).

[34] J. Anjos *et al.* (E691 Collaboration), Phys. Rev. D **46**, 1941 (1992).

[35] J.M. Link *et al.* (FOCUS Collaboration), Phys. Lett. B **575** 190 (2003).

[36] J.M. Link *et al.* (FOCUS Collaboration), Phys. Lett. B **610** 225 (2005).

[37] P.L. Frabetti *et al.* (E687 Collaboration), Phys. Lett. B **331** 217 (1994).

[38] J. Adler *et al.* (Mark III Collaboration), Phys. Lett. B **196** 107 (1987).

[39] S.U. Chung *et al.* (E852 Collaboration), Phys. Rev. D **65**, 072001 (2002).

[40] R. Kokoski and N. Isgur, Phys. Rev. D **35**, 907 (1987).

[41] J.H. Kühn and A. Santamaria, Z. Phys. C **48**, 445 (1990).

[42] J.L. Rosner, Phys. Rev. D **42**, 3732 (1990).

[43] G. Kramer and W.F. Palmer, Phys. Rev. D **45**, 193 (1992).

[44] M. Abiklim *et al.* (BES Collaboration), Phys. Lett. B **598** 149 (2004).

[45] M. Abiklim *et al.* (BES Collaboration), hep-ex/0605033.